DOI 10.17816/transsyst201843102-116

© X. H. Wang, Y. Jin, Y. Lin, D. Q. Lu, F. Qin
National Maglev Engineering Technology Center, Tongji University
(Shanghai, China)

SPEED INCREASING SCHEME BY USING 3000V DC POWER SUPPLY FOR LOW-SPEED MAGLEV

Background: Low-speed maglev is usually designed to run at a maximum speed of about 100~110 km/h, the system does not have any advantage to the traditional urban railway transportation system at the aspect of running speed.

Aim: Increase the speed of low-speed Maglev is an urgent task for future promotion.

Methods: This paper presents a speed increasing scheme by using 3000 V DC power supply instead of original 1500 V DC.

Results: Under this condition, the max output voltage of propulsion inverter could be doubled. For reason that the insulation of linear induction motor has enough margin, only small adjustment of motor is needed to adapt the doubled voltage.

Conclusion: To calculate the performance of low-speed maglev while using 3000 V DC, a T-model circuit of single-sided linear induction motor is built, and the result shows that the maximum running speed could be increased to over 160 km/h. This scheme provides a promising way for speed increasing, and it's a simple and economical approach to enhance the competitiveness of low-speed maglev.

Keywords: Low-speed maglev, Speed increasing, Maximum speed, Over voltage, SLIM, T-model circuit, 160 km/h, End-effect

INTRODUCTION

Low-speed maglev has made great progress in engineering application. Changsha maglev express, as the longest low-speed maglev line in the world, came into commercial operation in 2016 [1], and Beijing subway line S1 came into commercial operation at the end of 2017. These projects have verified that low-speed maglev has some merits when compared with the traditional urban railway, such as low noise, low vibration, excellent adaptability for smaller radius curves and larger slopes. As a result, several cities in China now plan to use low-speed maglev in urban transportation. But there still has a troublesome problem hard to overcome in the promotion of this technology. The suspending force of electromagnet has a limitation and couldn't be improved considerably, as a consequence, the passenger capacity of low-speed maglev is significantly lower than that of the metro and the light railway, which means this technology perhaps is more suitable for suburb transportation, which needs a higher running speed due to the longer distance

Received: 05.07.2018. Revised: 28.07.2018. Accepted: 01.10.2018.
Transportation Systems and Technology. 2018;4(3):102-116

doi: 10.17816/transsyst201843102-116

between stations. Therefore, if low-speed maglev couldn't significantly increase the running speed, its future would be pessimistic.

For decades, low-speed maglev in different countries is usually designed to run at a maximum speed of 100~110 km/h, which is similar to that of the metro. The Low-speed maglev line located at AICHI, Japan as the first commercial running maglev line in the world, based on the HSST 100L system has a maximum speed of 100 km/h [1]. The UTM-02 system of Korea put into service in 2016 at Incheon International Airport, has a maximum speed of 110 km/h [3]. Changsha maglev express's highest speed is 100 km/h [2]. However, there is still no proper rail transportation form to fill the blank of 140~200 km/h, neither do maglev, nor metro.

As mentioned above, to speed up the low-speed maglev to the so called 'medium-speed maglev', performance studies of single-sided linear induction motor (SLIM) of low-speed maglev is necessary. Reference [3] provided one useful function expression $f(q)$ according to the SLIM secondary eddy current average value. This paper supposed that the air-gap flux linkage increased in the exponential function form from the entrance end to the exit end, it is affected by the SLIM running speed, secondary resistance and some other structure parameters. The per-phase simplified model can be used to calculate the output thrust force, efficiency conveniently. Reference [4] deduced a two-axis models to predict the SLIM dynamic performance, which can be applied in vector control of direct torque control. Reference [5] derived an equivalent circuit model from the pole-by-pole method, based on the winding functions of the SLIM primary winds. Reference [6] based on the results of reference [5], divided the SLIM air-gap flux density into three components. Then these three components were derived and get the inductance, secondary resistance and other parameters. A field theory analysis is performed to build a combined-parameter SLIM model in Reference [7]. The paper estimated the end-effect, the skin effect, and the back-iron saturation. Several different models were built from the electromagnetic relation in the air gap through a Fourier-series approach [8, 9, 10]. However, there are very few researches focused on speed increasing scheme for the SLIM of low-speed maglev. CRRC Zhuzhou Institute LTD. China is now developing on 'low-speed maglev 2.0' whose maximum speed is designed at 160 km/h. The primary approach used in the project is to redesign the linear induction motor by extending the length and width of iron cores so as to improve the thrust force [13]. Consequently, the motor is getting much heavier, and this kind of design challenges the electromagnetic suspending system, weakens the adaptability of line curve. Furthermore, the vehicle structure has to be redesigned totally. Obviously, there are tremendous works need to be done before finally achieving the goal speed.

This article presents a different way for speed increasing. As 3000 V DC is another electric tracking voltage in IEC standard, 3000 V DC power supply was

Received: 05.07.2018. Revised: 28.07.2018. Accepted: 01.10.2018.
Transportation Systems and Technology. 2018;4(3):102-116

doi: 10.17816/transsyst201843102-116

adopted instead of original 1500 V DC. Then the output voltage of the vehicular propulsion inverter was doubled. A preliminary analysis was performed to confirm the motor insulation has enough margin to endure the doubled voltage. Therefore, little modification is needed for the linear motor and vehicle structures. The key benefits of this approach is that motor voltage can keep rising with speed for longer time, and appearance of the constant power area is delayed. A mathematical model of SLIM based on T-model considering the end-effect was built to calculate the performance of the propulsion system, and the result showed that the maximum running speed exceeded 165 km/h when 3 sections formation adopted. The result can contribute to the exploration of a new feasible scheme for the application of 'medium-speed maglev'.

MODELING OF THE SLIM

The SLIM used in Low-speed maglev is shown in Fig. 1. The SLIM primary can be simply regarded as rotary cut-open stator and then rolled flat. The Secondary, similar with rotary induction motor (RIM) rotor, often consists of a sheet conductor, such as copper or aluminum, with a solid back iron acting as return path for the magnetic flux. The thrust force corresponding to the RIM torque can be produced by the reaction between the air-gap flux density and the eddy current in the secondary sheet [15].

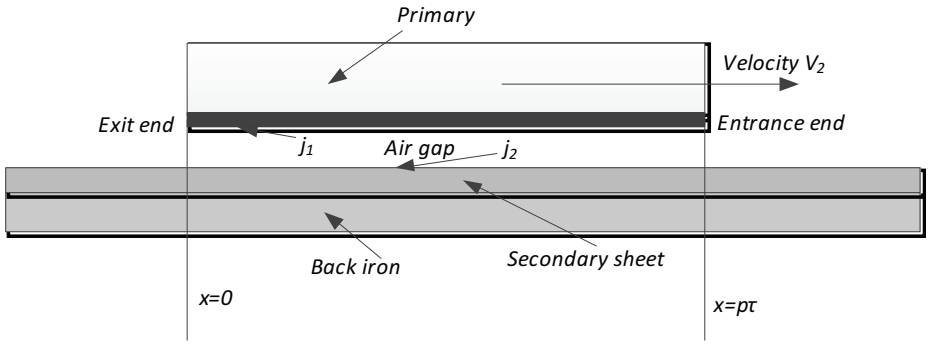

Fig. 1. Longitudinal structure view of SLIM

The SLIM special structure means that its performance is a little different from that of an RIM. As we know, in the RIM, an accurate equivalent circuit model can be derived easily by simplifying the geometry per pole. Unfortunately, it is not as straightforward as for RIM to gain the equivalent circuit for a SLIM.

In Fig. 1 v_2 is the primary moving speed, j_1 is the primary equivalent current, and j_2 is the secondary equivalent current. In terms of 1-D analysis, we can calculate the phase currents and excitation voltages. The air gap flux linkage can be obtained

Received: 05.07.2018. Revised: 28.07.2018. Accepted: 01.10.2018.
Transportation Systems and Technology. 2018;4(3):102-116

doi: 10.17816/transsyst201843102-116

using Maxwell's field equations and solved using the complex power method with a conformal transformation which considers the effects of the half-filled slots, magnetic saturation, and back-iron resistance. By using the equal complex power relationship between the magnetic field and the electrical circuit, we can obtain several circuit parameters, such as mutual inductance L_m, secondary resistance R_r, primary leakage inductance L_{1s}, secondary leakage inductance L_{1r}, longitudinal end effect coefficients C_r and C_x. The comprehensive derivations of the four coefficients can be referred to [15]. The T-model equivalent circuit is shown in Fig. 2, where the secondary equivalent resistance R_r consists of the secondary conducting sheet resistance R_{2sheet} and the secondary back iron R_{2back}. Some brief conclusions are summarized in the following paragraphs.

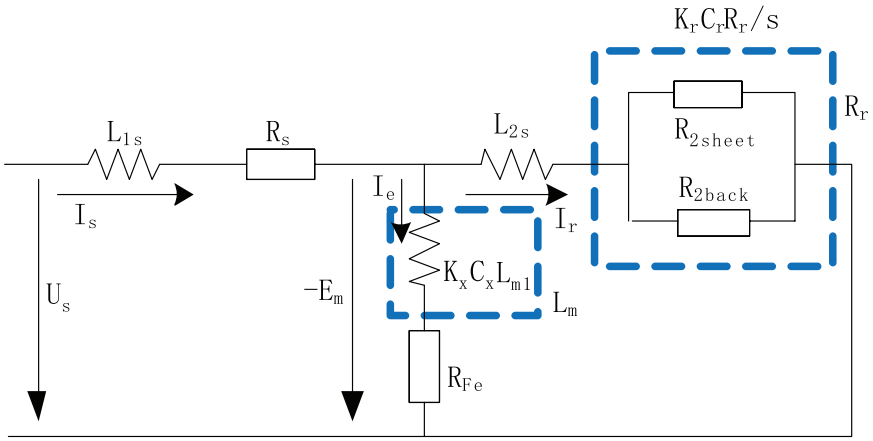

Fig. 2. The T-model circuit for SLIM

The longitudinal end effect coefficients K_r and K_x are denoted by

$$K_r = \frac{sG}{\left(2p_e\tau\sqrt{1+(sG)^2}\right)}\frac{C_1^2+C_2^2}{C_1} \tag{1}$$

$$K_x = \frac{1}{\left(2p_e\tau\sqrt{1+(sG)^2}\right)}\frac{C_1^2+C_2^2}{C_1} \tag{2}$$

where τ is the primary pole pitch, and p_e is the number of pole pairs. C_1 and C_2 are functions of the slip and machine structure parameters, described as follows,

$$\begin{aligned} C_1 = {} & p\tau\cos\delta_s - N_L \times [\alpha_1^{-1}e^{-p\tau/\alpha_1}\sin(\delta_s-\beta+S_L p\tau) \\ & + S_L e^{-p\tau/\alpha_1}\cos(\delta_s-\beta+S_L p\tau) \\ & - \alpha_1^{-1}\sin(\delta_s-\beta) - S_L\cos(\delta_s-\beta)] \end{aligned} \tag{3}$$

$$\begin{aligned} C_2 = {} & p\tau\sin\delta_s - N_L \times [-\alpha_1^{-1}e^{-p\tau/\alpha_1}\cos(\delta_s-\beta+S_L p\tau) \\ & + S_L e^{-p\tau/\alpha_1}\sin(\delta_s-\beta+S_L p\tau) \\ & + \alpha_1^{-1}\cos(\delta_s-\beta) - S_L\sin(\delta_s-\beta)] \end{aligned} \tag{4}$$

Received: 05.07.2018. Revised: 28.07.2018. Accepted: 01.10.2018.
Transportation Systems and Technology. 2018;4(3):102-116

doi: 10.17816/transsyst201843102-116

Parameters in (1) and (2) are calculated as below,

$$\begin{aligned} &\alpha_1 = \frac{\tau g_e}{g_e X - \mu_0 \sigma_e v_2} \\ &S_L = k - \frac{\pi}{\tau_e},\ M_L = (\alpha_1^{-1})^2 + S_L^2 \\ &N_L = \frac{\alpha_1 \pi \tau_e}{M_L \tau \sqrt{\tau_e^2 + (\pi \alpha_1)^2}} \\ &\delta_s = \tan^{-1}\left(\frac{1}{S_L G}\right),\ \beta = \tan^{-1}\left(\frac{\pi \alpha_1}{\tau_e}\right) \end{aligned} \tag{5}$$

For the existence of half-filled slots in the primary ends, the expression of the primary equivalent sheet current J_1 can be divided into three regions, i.e., entrance half-filled, full-filled, and exit half-filled slots. Then, the expressions of the air-gap flux density can be gained. According to the electric machinery theory and complex power conversion algorithm, the air-gap effective electromotive force E_m, air-gap reactive power Q_3, secondary active power P_2, mutual inductance and secondary resistance can be deduced by taking the half-filled slots into consideration. By the comparison of these expressions without half-filled slots, the number of equivalent pole pairs p_e is expressed by

$$p_e = \frac{(2p-1)^2}{4p - 3 + \varepsilon/(m_1 q)} \tag{6}$$

where p is the actual number of the pole pairs, m_1 is the number of primary phases, q is the number of coil sides per phase per pole, and ε is the length of the short pitch.

The transversal-edge-effect coefficients are calculated by

$$C_r = \frac{sG[R_e^2[T] + I_m^2[T]]}{\mathrm{Re}[T]} \tag{7}$$

$$C_x = \frac{[R_e^2[T] + I_m^2[T]]}{\mathrm{I}_m[T]} \tag{8}$$

where T is the function of the slip, goodness factor, and motor structure parameters, Re and I_m are the real and imaginary parts of complex T respectively. Here, T is expressed by

$$T = j\left[\gamma^2 + (1-\gamma^2)\frac{\lambda}{0.5 l_\delta \alpha} th(0.5 l_\delta \alpha)\right] \tag{9}$$

where α is the ratio of c to τ, γ and λ can be obtained by

$$\lambda = \frac{1}{1 + \frac{1}{\gamma} th(0.5 l_\delta \alpha) th[0.5K(c_2 - l_\delta)]} \tag{10}$$

Received: 05.07.2018. Revised: 28.07.2018. Accepted: 01.10.2018.
Transportation Systems and Technology. 2018;4(3):102-116

doi: 10.17816/transsyst201843102-116

$$R^2 = \frac{1}{1 + jsG} \tag{11}$$

where K is the function of the slip and motor structure parameters and c_2 is the width of the secondary sheet.

The five parameters in T-model circuit, respectively named as the primary resistance R_s, primary leakage inductance L_{1s}, secondary resistance R_r, secondary leakage inductance L_{1r}, and exciting inductance L_m, can be calculated as follows.

The primary resistance R_s is

$$R_s = \rho_{Cu} \times 2 l_{av} W_1 / S_{cu} \tag{12}$$

where ρ is the resistivity of copper, *lav* is half the average length of the primary winding coil, W_1 is the number of turns in series of the primary per phase, and S_{Cu} is the effective cross-sectional area of the primary winding conductor.

The primary leakage inductance L_{1s} is

$$L_{1s} = 0.025 W_1^2 \frac{l_\delta}{q} \left(\frac{\lambda}{p} + \frac{\lambda_t + \lambda_e + \lambda_d}{p_e} \right) \tag{13}$$

where λ_s is the primary slot leakage magnetic conductance, λ_e is the primary winding end leakage magnetic conductance, and λ_d is the primary harmonic leakage magnetic conductance.

The secondary resistance is composed of two parts, which is sheet and back resistance, because the flux can penetrate through the aluminum or copper sheet and enter the back iron. The depth of the flux density into the back iron d_{Fe} is

$$d_{Fe} = \sqrt{\frac{2\rho_{Fe}}{s\omega_e \mu_{Fe}}} \tag{14}$$

where ρ_e is the back iron resistivity, μ_{Fe} is the permeability of the back iron, and ω_e is the primary synchronous angular frequency. The resistance of the secondary conducting sheet R_{2sheet} is

$$R_{2sheet} = 4 m_1 \rho_{sheet} \frac{(W_1 K_{W1})^2}{2 p_e} \frac{l_\delta}{d\tau} \tag{15}$$

where ρ_{sheet} is the resistivity of the secondary conductance sheet and K_{W1} is the primary winding coefficient.

The resistance of the secondary back iron R_{2back} is

$$R_{2back} = 4 m_1 \rho_{Fe} \frac{(W_1 K_{W1})^2}{2 p_e} \frac{l_\delta}{d_{Fe} \tau} \tag{16}$$

Therefore, the secondary equivalent resistance R_r is

$$R_r = \frac{R_{2sheet} R_{2back}}{R_{2sheeet} + R_{2back}} \tag{17}$$

Received: 05.07.2018. Revised: 28.07.2018. Accepted: 01.10.2018.
Transportation Systems and Technology. 2018;4(3):102-116

doi: 10.17816/transsyst201843102-116

The secondary leakage reactance is

$$L_{1r} = \frac{R_r}{2\pi f_s s} B_1 sh(2Kd) \tag{18}$$

where f_s is the primary frequency and B_1 is the function of the slip, primary frequency, and machine structure parameters.

The exciting inductance is

$$L_{m1} = 4m_1 \mu_0 (W_1 K_{W1})^2 \frac{l_\delta V_s}{4\pi^2 f_s g_e p_e} \tag{19}$$

where V_s is the synchronous velocity of the primary side and g_e is the equivalent air-gap width.

The iron loss in the SLIM is composed of the primary yoke, primary tooth, and secondary back iron losses. These three parts can be calculated as follows.

The primary yoke iron loss P_{Fe} is

$$P_{Fe} = P_{10/50} B_y^2 \left(\frac{f_s}{50}\right)^{1.3} W_y \tag{20}$$

The primary tooth iron loss P_{Fe} is

$$P_{Feb} = P_{10/50} B_b^2 \left(\frac{sf}{50}\right)^{1.3} W_b \tag{21}$$

Hence, the total iron loss P_{Fe} is

$$P_{Fe} = P_{Fet} + P_{Fey} + P_{Feb} \tag{22}$$

In (20)–(21), $P_{10/50}$ is the iron loss value under 1.0 T and 50 Hz; B_y, B_t and B_b are the primary yoke, primary tooth and secondary back iron flux densities respectively; W_y, W_t and W_b are the primary yoke, primary tooth and secondary back iron weights respectively; and *sf* is the slip frequency in the secondary. According to the electromagnetic design methods in [11], B_y, B_t and B_b can be calculated as follows,

$$B_y = \sqrt{2}\,\phi_y / (2l\delta K_{lam} h_y) \tag{23}$$

$$B_t = B_g t_1 / (K_{lam} t_2) \tag{24}$$

$$B_b = \phi_g / (c_2 K_{lam} h_b) \tag{25}$$

where ϕ_g is the flux root-mean-square value per pole pair, K_{lam} is the silicon steel stacking factor, h_y is the primary height, B_g is the leakage air-gap flux density, t_1 is the pitch of the primary teeth, t_2 is the width of the primary teeth, and h_y is the height of the secondary back iron.

The iron loss resistance R_{Fe} in series with the excitation branch can be calculated by

$$R_{Fe} = P_{Fe} / I_e^2 \tag{26}$$

where I_e is the field current.

Received: 05.07.2018. Revised: 28.07.2018. Accepted: 01.10.2018.
Transportation Systems and Technology. 2018;4(3):102-116

doi: 10.17816/transsyst201843102-116

Besides the edge-effect, the skin-effect, big air-gap and thick secondary conductor are also very influential to SLIM's performance when running at a relative high speed. In order to get more accurate circuits, a skin-effect coefficient is calculated to adjust the secondary leakage inductance by using 2-D electromagnetic field theory in [15]. The skin-effect coefficient is

$$k_f = \frac{1 + (B\sinh 2k\delta)^2}{A[1 + (B\sinh 2kd)^2]} \tag{27}$$

where d is the thickness of secondary conductor sheet. Coefficients A and B are calculated as follows

$$A = \cosh^2 k\delta' + \left(\frac{k\rho_{sheet} shnhk\delta'}{s\omega_e \mu_0 d}\right)^2 \tag{28}$$

$$B = \frac{s\omega_e \mu_0 d}{2k\rho_{sheet}}\left[1 + \left(\frac{k\rho_{sheet}}{s\omega_e \mu_0 d}\right)^2\right] \tag{29}$$

where s is the slip of SLIM, μ_0 is the air relative permeability, δ' is the equivalent air-gap.

PERFORMANCE CALCULATION

After approximate analysis of the four coefficients and parameter calculations, the SLIM T-model equivalent circuit indicated in Fig. 2 is got. The model is similar to that of RIM. The influence of longitudinal and transversal end-effect and half-filled slots can be estimated by corresponding coefficients. Therefore, it is very convenient to analyze the performance of the SLIM in a similar way to RIM. Main performance index calculation is showed as follows.

The secondary current is

$$I_r = I_s \times \frac{R_{Fe} + j\omega_e L_m}{R_{Fe} + j\omega_e L_m + R_r + j\omega_e L_{2r}} \tag{30}$$

The output mechanical power is

$$P_m = I_r^2\left(\frac{1-s}{s} K_r C_r R_r\right) \tag{31}$$

The power factor is

$$\cos\varphi = \cos\left(\operatorname{atan}\left(\frac{\operatorname{Im}\left(R_s + j\omega_e L_{1s} + \frac{(R_{Fe} + j\omega_e L_m)(R_r + j\omega_e L_{2r})}{R_{Fe} + j\omega_e L_m + R_r + j\omega_e L_{2r}}\right)}{\operatorname{Re}\left(R_s + j\omega_e L_{1s} + \frac{(R_{Fe} + j\omega_e L_m)(R_r + j\omega_e L_{2r})}{R_{Fe} + j\omega_e L_m + R_r + j\omega_e L_{2r}}\right)}\right)\right) \tag{32}$$

The input voltage of the SLIM is

$$U_s = I_s \times \left(R_s + j\omega_e L_{1s} + \frac{(R_{Fe} + j\omega_e L_m)(R_r + j\omega_e L_{2r})}{R_{Fe} + j\omega_e L_m + R_r + j\omega_e L_{2r}}\right) \tag{33}$$

Received: 05.07.2018. Revised: 28.07.2018. Accepted: 01.10.2018.
Transportation Systems and Technology. 2018;4(3):102-116

doi: 10.17816/transsyst201843102-116

The efficiency of the SLIM is

$$\eta - P \ /(U \ I \ \cos\varphi) \tag{34}$$

The output thrust force of single SLIM is

$$F_x = P_m / v_2 \tag{35}$$

INSULATION ANALYSIS

When 3000 V DC is adopted as input voltage from the power rail, the maximum output voltage of the vehicular propulsion inverter doubles to 2200 V AC, each SLIM's maximum input voltage rises to 440 V AC, and the maximum phase voltage is 254 V. Through the control of the inverter, the maximum input current is still limited to 300 A, therefore main size of SLIM wouldn't change a lot, the mechanical interface could keep unchanged.

From the design experience, we know that usually the weakest part of machine insulation system is the turn-to-turn insulation. At this point, the test line in Shanghai and the commercial line in Changsha all use polyimide film (PI) as the main turn-to-turn insulation. 2 layers of PI using 1/2 lapping method wrapped up around the primary aluminum winding coil, each layer's thickness is 0.06mm and the total turn-to-turn insulation thickness is 0.12 mm. The insulation strength of the common industrial PI reaches 200 kV/mm [16], the corona-resistance reaches about 2 kV/mm. On condition of using PI thickness of 0.12 mm, the insulation strength of the primary coil is no less than 20 kV and corona-resistance is no less than 2 kV. The insulation capability is significantly higher than the doubled input voltage of SLIM. Even when the voltage of the first turn of motor could reach nearly 80 % of terminal voltage in a PWM control system [17], there is still enough voltage margin to the insulation limitation.

SLIP FREQUENCY AND MOTOR PARAMETERS

Because the SLIM of low-speed maglev has quite different structure with that of RIM [12],the control strategy is also quite different. Considering the unique phenomenon of normal force, constant slip frequency control strategy is chosen to minimize the influence on suspending control [17]. But the reference slip frequency must be confirmed before using constant slip frequency control.

Set slip frequency as the independent variable and normal force as the dependent variable, the relation curve is show in Fig. 3. The figure shows that the normal force is very close to zero when slip frequency equals to 12 Hz. Hence, 12 Hz is selected as the reference slip frequency in performance calculation.

Received: 05.07.2018. Revised: 28.07.2018. Accepted: 01.10.2018.
Transportation Systems and Technology. 2018;4(3):102-116

doi: 10.17816/transsyst201843102-116

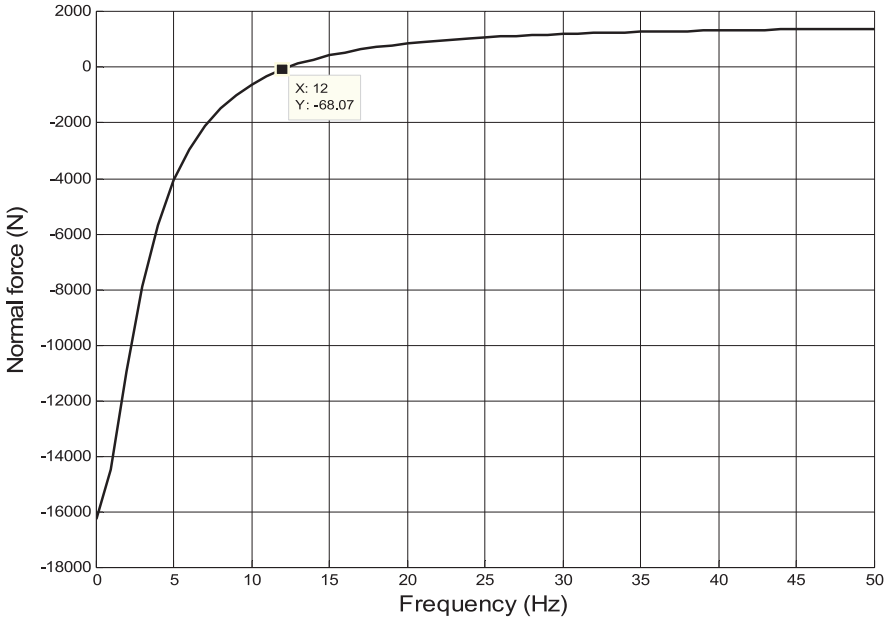

Fig. 3. Normal force curve at different slip frequency

After confirming the slip frequency, all parameter could finally be substituted into T-model equations. The main parameters of the SLIM in this paper are listed in Table 1, and the vehicle configurations are listed in Table 2.

Table 1. Main parameter of the SLIM

Items	Unit	Value
Width of primary iron core	mm	190
Pole pairs		9/2
Silicon steel sheet length	mm	1783
Gap flux	T	0.1467
Rated frequency	Hz	42.5
Pole pitch	mm	202.5
Secondary sheet thickness	mm	4
Width of secondary sheet	mm	200
Mechanical air gap	mm	10
Primary slots number		79
Slot width	mm	16.1
Tooth width	mm	6.4
Series turns per phase		96

Table 2. Vehicle configuration

Motor number per section	10
Section number	3
Full loaded mass per section (kg)	30 000
Motors in series	5
Paralleling motor branches	2
Maximum inverter current(A)	300

Received: 05.07.2018. Revised: 28.07.2018. Accepted: 01.10.2018.
Transportation Systems and Technology. 2018;4(3):102-116

doi: 10.17816/transsyst201843102-116

RESULTS AND DISCUSSION

This paper focus on speed increasing of low-speed maglev, so the most important performance index is maximum running speed. T-model circuit is used to calculate the propulsion thrust force at each v_2 of primary side, which is the running speed of maglev vehicle too. It's easy to find that the cross point of thrust force curve and resistance force curve is the ultimate running speed.

In order to indicate the variation trend of running performance when adopting different over voltage mode, we set the highest voltage 2 times to the current rated voltage, that's 2.0 pu. Then set another 5 uniform distributed voltage grades with 0.2 pu step, from 1.0 to 2.0 pu. Calculation results are illustrated in Fig. 4.

From the results we can draw some preliminary findings,

- Maximum running speed at 1.0 pu condition is about 108 km/h, the turning point of thrust force curve is around 40 km/h and the start acceleration is about 1.15 m/s^2, all these results accord with the design index and the actual testing results. The fact proved that the calculation model built in this article is accuracy and could be used to verify the over voltage performance.
- Voltage has great influence on the maximum speed, when the highest input voltage of the SLIM doubled, maximum speed increased over 50 %. Taken 3 sections formation as example, the maximum speed increased from 108 km/h to 166 km/h.

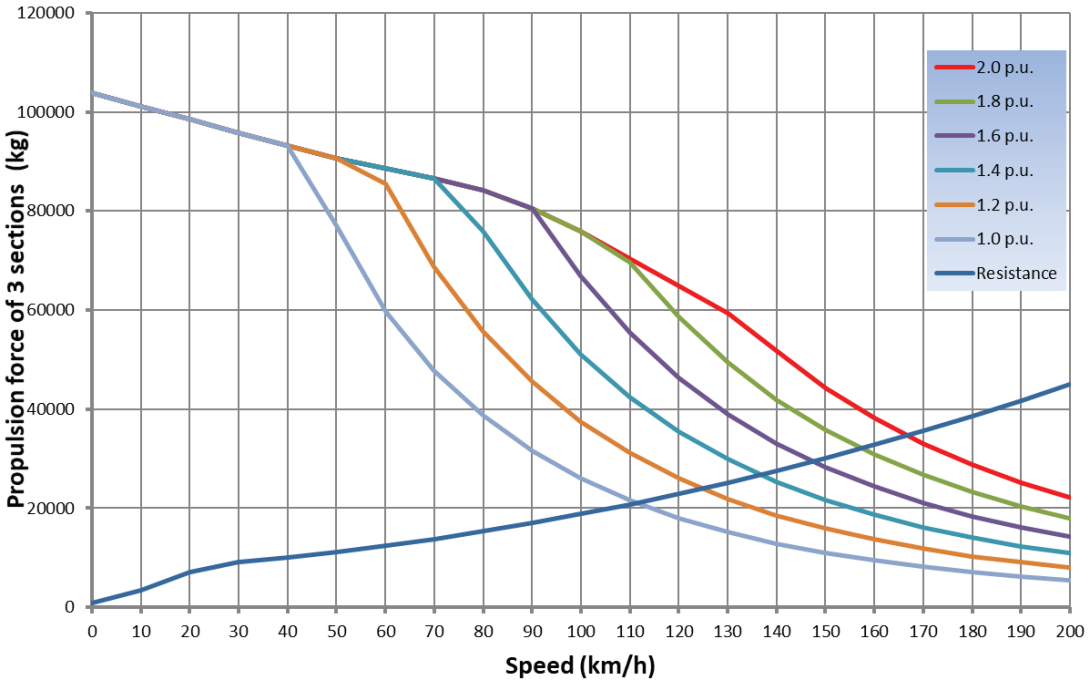

Fig. 4. Thrust force versus resistance force

Received: 05.07.2018. Revised: 28.07.2018. Accepted: 01.10.2018.
Transportation Systems and Technology. 2018;4(3):102-116

doi: 10.17816/transsyst201843102-116

- The appearance of constant power area of the SLIM is significantly delayed with voltage increased, the higher voltage increased, the later SLIM comes into constant power area;
- With voltage doubled, the curve of propulsion force drops slightly, and there is almost no turning point on the curve. From this we can see that the end-effect, especially longitudinal end-effect significantly affects the performance of the SLIM when high speed running.

Acceleration ability is also an important performance index. To indicate the acceleration ability, we assumed that vehicle running at a straight line without any turning curves and slopes, then record the distances and times when vehicle get the maximum speed, the results are listed in Table 3. When taking the look at 2.0 pu condition column, although the goal speed of 160 km/h is achieved, the acceleration distance is about 2.5 km, it's too long if the station spacing is less than 5 km. Furthermore, there must be some speed limitations when applied to actual running line with smaller radius curves and slopes, the acceleration distance would surely be much longer than figures in Table 3.

Table 3. Performance of the 3 sections formation vehicle

Index	2.0/pu	1.8/pu	1.6/pu	1.4/pu	1.2/pu	1.0/pu
Maximum speed (km/h)	166	157	146	135	122	108
Acceleration time (s)	298	288	272	265	252	245
Acceleration distance (m)	2520	2337	2058	1879	1623	1404
Average acceleration (m/s^2)	0.56	0.54	0.54	0.51	0.48	0.44

In Fig. 5, the power factor and motor efficiency curve on condition of 2.0 pu are drew. Efficiency rises from 0.4 to near 0.8 with speed increasing, and power

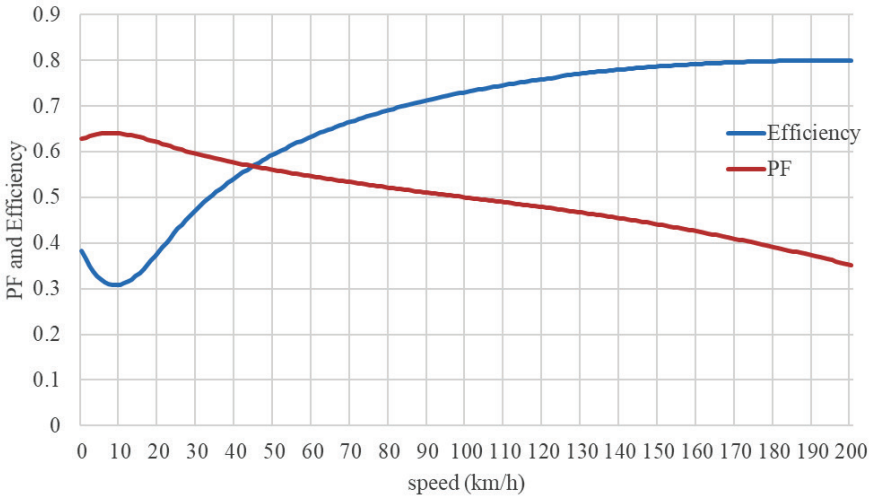

Fig. 5. Efficiency and PF of the SLIM at 2.0 pu

Received: 05.07.2018. Revised: 28.07.2018. Accepted: 01.10.2018.
Transportation Systems and Technology. 2018;4(3):102-116

doi: 10.17816/transsyst201843102-116

factor drops slightly from about 0.6 to under 0.4. Both index is relatively a bit lower than that of RIM, mainly because of characteristic of induction motor. Besides, big air-gap and more field excitation loss at over voltage mode deteriorate the power factor.

CONCLUSION

This paper presented a speed increasing scheme for low-speed maglev by adopting 3000 V DC power supply. After building a T-model circuit in consideration of end-effect, analysis of the SLIM performance is made. Results show that increasing the input voltage of the SLIM is an efficient way to increase the maximum speed of low-speed maglev. Calculation of thrust force curve indicates a 3 sections formation vehicle can get the highest speed over 165 km/h on condition of 2.0 pu voltage.

This voltage increasing way rarely needs adjustment or redesign to the SLIM, the mechanical interface of the SLIM could remain unchanged, so do the structure of vehicle. It's an economical way to increase running speed largely. However, the SLIM of low-speed maglev is originally designed to run at the maximum speed of 100~110 km/h, the performance is far from perfect when running at over voltage mode, for example, the acceleration ability is fairly weak when speed exceeds 100 km/h, and acceleration distance is too long to meet the demands of actual line. Therefore, further research is necessary to optimize the performance of the SLIM and take full advantage of the potentiality of increased terminal voltage.

References

1. Yasuda Y, Fujino M, Tanaka M, et al. The first HSST Maglev Commercial Train in Japan. Proceedings of the 18th international conference on magnetically levitated systems and linear drives; 2004 Oct. 26–28, Shanghai, China.
2. Shin BC, Park DY, Han HS. Korea's First Urban Maglev System. Proceedings of the 22th International conference on magnetically levitated systems and linear drives; 2014 Sep.28–Oct.2, Rio de Janeiro, Brazil.
3. Duncan J. Linear Induction Motor-equivalent-circuit Model, IEE Proceedings B (Electric Power Applications). 1983;130(1):51-57. doi: 10.1049/ip-b.1983.0008
4. Kang G, Nam K. Field-oriented Control Scheme for Linear Induction Motor with the End Effect. IEE Proceedings-Electric Power Applications. 2005;152(6):1565-1572. doi: 10.1049/ip-epa:20045185
5. Lipa TA, Nondahl TA. Pole by Pole d-q Model of a Linear Induction Machine. IEEE Transactions on Power doi: https://doi.org/10.1109/tpas.1979.319448
6. Apparatus and Systems. 1979;PAS-98(2):629-642. doi: 10.1109/tpas.1979.319448

Received: 05.07.2018. Revised: 28.07.2018. Accepted: 01.10.2018.
Transportation Systems and Technology. 2018;4(3):102-116

doi: 10.17816/transsyst201843102-116

7. Lu CA. A New Coupled-circuit Model of a Linear Induction Motor and Its Application to Steady-state Transient Dynamic and Control Studies [dissertation]. Kingston, Ontario: Queen's University; 1993.
8. Idir K, Dawson GE, Eastham AR. Modeling and Performance of Linear Induction Motor With Saturable Primary. Conference Record of the 1991 IEEE Industry Applications Society Annual Meeting; 1991 28 Sept. 4 Oct., Dearborn, MI, USA. New York: IEEE, New York, 1993. doi: 10.1109/ias.1991.178147
9. Higuchi T, Nonaka S, Ando M. On the Design of High Efficiency Linear Induction Motors for Linear Metro. *Electrical Engineering in Japan*. 2001;137(2):36-43. doi: 10.1002/eej.1086
10. Xu W. Research On the Performance of Single-sided Linear Induction Motor. IEEE International Electric Machines and Drives Conference; 2007 3–5 May; Antalya, Turkey. Piscataway: IEEE, 2007.
11. Nonaka S. Investigation of equations for calculation of secondary resistance and secondary leakage reactance of single sided linear induction motors. *Electrical Engineering in Japan*. 1997;117(5):616-621.
12. Poloujadoff M. The Theory of Linear Induction Machinery. 1st ed. Clarendon: Oxford University Press; 1980, 273 p.
13. Wang K, Shi LM, He JW, Li YH. A Decoupling Control of Normal-and-thrust Forces in Single-sided Linear Induction Motor. Proceedings of the CSEE. 2009;29(06):100-104.
14. Yan JP, Wang DW. Prospect Analysis of Application the Low-speed Maglev System in Changsha. *Underground Engineering and Tunnels*. 2016;4:29-31.
15. Deng JM, Liu YM, Chen TF. Discussion on Facing Higher Speed Engineering Applications of Short-primary Linear Induction Motor. *Electric Locomotives & Mass Transit Vehicles*. 2017;40(4):1-5.
16. Long XL. *Theory and Electromagnetic Design Method of Linear Induction Motor.* 1st ed. Beijing: Science Press; 2006.
17. Rotating electrical machines-Part 18-1: Functional evaluation of insulation systems – General guidelines. IEC 60034-18-1. Edition 2.0 2010-03.
18. Zhang LL. Study on Premature Fai1ure Mechenism of PWM Inverter-Fed Traction Motor [dissertation]. Chengdu (Sichuan): Sounthwest Transportation University: 2004.
19. Deng JM, Chen TF, Tang JX, Tong LS. Optimum Slip Frequency Control of Maglev Single-sided Linear Induction Motors to Maximum Dynamic Thrust. Proceedings of the CSEE. 2013;12:123-130.

Information about the authors:
Wang Xiaohua, Master degree, assistant researcher; Tongji university, Caoan Road, Jiading district, Shanghai, China.
ORCID: 0000-0003-1061-6370;
E-mail: wangxiaohua@tongji.edu.cn

Jin Yu, Master degree, assistant researcher;
E-mail: jinyu@tongji.edu.cn

Received: 05.07.2018. Revised: 28.07.2018. Accepted: 01.10.2018.
Transportation Systems and Technology. 2018;4(3):102-116

doi: 10.17816/transsyst201843102-116

Lin Ying, Master degree, assistant researcher;
ORCID: 0000-0002-2270-272X
E-mail: carfieldlin@tongji.edu.cn

Lu Diqiang, Doctor degree, assistant researcher;
E-mail: ludiqiang@tongji.edu.cn

Qin Feng, Doctor degree, assistant researcher;
E-mail: qinfeng@tongji.edu.cn

To cite this article:
Wang XH, Yu J, Lin Y, et al. Speed Increasing Scheme by Using 3000 V DC Power Supply for Low-Speed Maglev. *Transportation Systems and Technology.* 2018;4(3):102-116. doi: 10.17816/transsyst201843102-116

Received: 05.07.2018. Revised: 28.07.2018. Accepted: 01.10.2018.
Transportation Systems and Technology. 2018;4(3):102-116

doi: 10.17816/transsyst201843102-116